THE AMERICAN SOCIETY OF MECHANICAL ENGINEERS
345 E. 47th St., New York, N.Y. 10017

94-GT-94

HEAT TRANSFER TO ROTATING TURBINE BLADES IN A FLOW UNDISTURBED BY WAKES

T. Garside, R. W. Moss, and R. W. Ainsworth
Department of Engineering Science
University of Oxford
Oxford, United Kingdom

S. N. Dancer and M. G. Rose
Rolls-Royce plc
Derby, United Kingdom

ABSTRACT

The flow over the high pressure blades of a gas turbine is disturbed by wakes and shock waves from the nozzle guide vanes upstream. These disturbances lead to increased heat transfer to the blade surfaces, the accurate prediction of which is an essential stage in the design process.

The Oxford Rotor experiment consists of a highly instrumented 0.5 m diameter shroudless turbine which is supplied with air from a piston tube during the 200 ms run time and simulates realistic engine Mach and Reynolds numbers. Previous experiments have measured blade surface pressures and heat transfer rates, and compared them with similar data from linear cascades.

The present work is designed to enable the accuracy of rotation terms in computational fluid dynamics (CFD) calculations to be assessed, by providing heat transfer data from the rotating frame in the absence of wakes. Flow disturbances were avoided by removing the nozzle guide vanes, the correct angle of incidence onto the rotor blades being achieved by rotating the rotor in the reverse direction. Blade surface heat fluxes were measured using thin film gauges. In the absence of the usual blade-passing fluctuations, the root-mean-square fluctuation in heat flux was typically only 7% of the DC level.

Nusselt numbers are compared with cascade data and CFD predictions from both a three-dimensional viscous Navier-Stokes equation solver and a two-dimensional boundary layer prediction. The low inlet turbulence level produced a long laminar region on the suction surface followed by sudden transition. CFD predictions of Nusselt number on this surface were very sensitive to the choice of boundary layer state, and the experimental level was approximately mid-way between predictions with a transitional intermittency distribution and those with a turbulent distribution. On the pressure surface the levels were approximately 25% below predicted levels, and possible reasons for this are considered.

NOMENCLATURE.

C_{ax}	blade axial chord, mm.
k	conductivity of air, evaluated at wall temperature.
Nu	Nusselt number
$\dot{q}$	heat flux, W/m^2
PTFE	polytetrafluoroethylene
Re	Reynolds number based on rotor-relative conditions, exit Mach number and axial chord.
S	surface length from stagnation point to trailing edge along pressure or suction surfaces.
T	temperature, K.
x	axial distance from leading edge.
X	perimeter length from stagnation point to gauge positions.
σ	boundary layer fractional intermittency level.

Subscripts:

$_0$	recovery temperatures
$_{rel}$	in blade-relative frame
$_w$	at wall conditions

INTRODUCTION.

The Oxford Rotor experiment (Ainsworth et al, 1988a) was designed both to provide an insight into the phenomena responsible for heat transfer in gas turbines and to create data against which computational fluid-dynamic (CFD) codes could be evaluated. Blade surface heat flux levels are measured using thin-film gauges.

The development of accurate CFD codes requires all the phenomena that affect heat transfer to be understood and quantified. At present, the effects of flow unsteadiness are usually incorporated into time-steady calculations by specifying

Presented at the International Gas Turbine and Aeroengine Congress and Exposition
The Hague, Netherlands — June 13–16, 1994

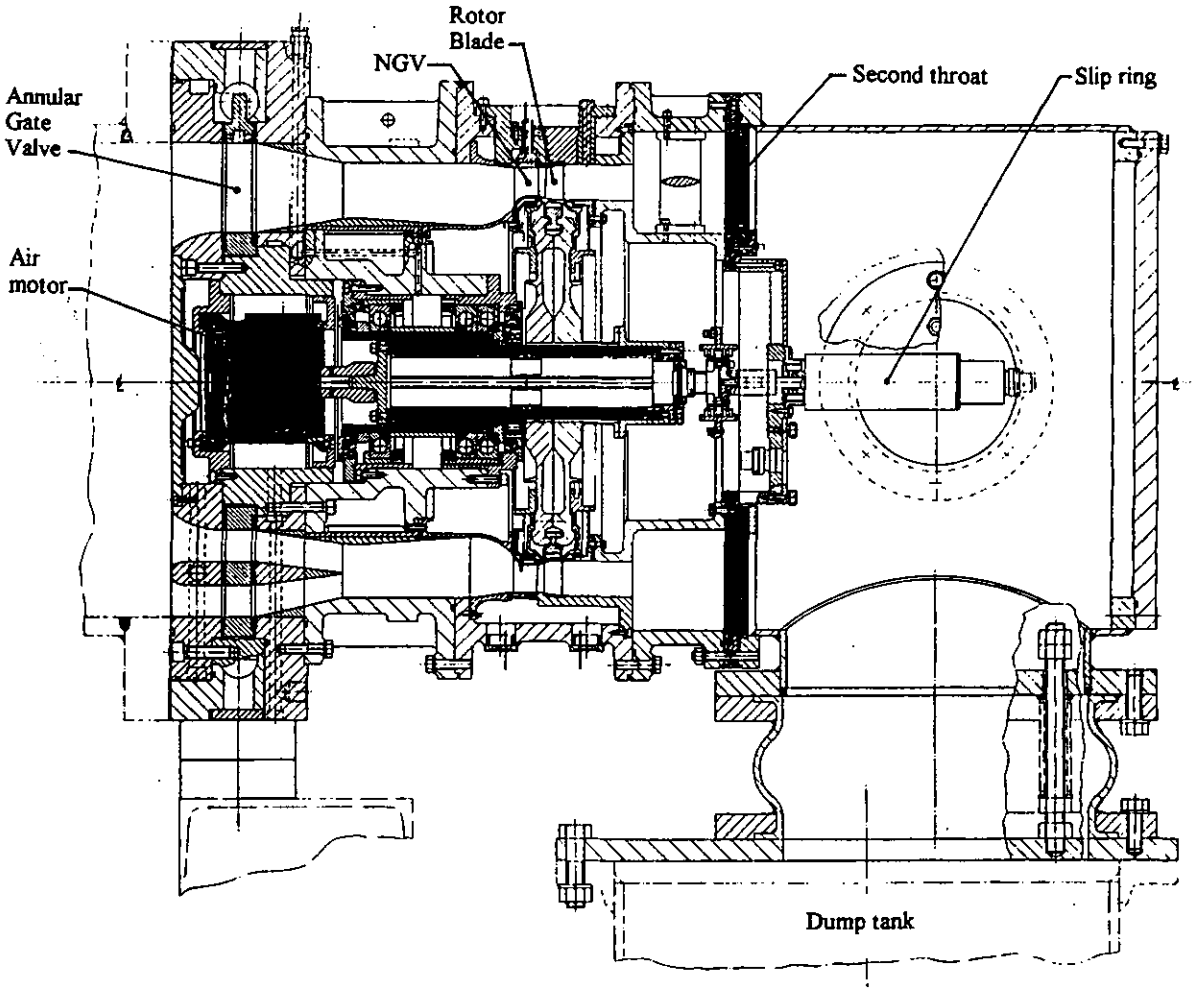

FIGURE 1. GENERAL ASSEMBLY OF THE WORKING SECTION OF THE OXFORD ROTOR PRIOR TO REMOVAL OF GUIDE VANES FOR REVERSE ROTATION.

an empirical high turbulence level which past experience has found to raise the heat transfer to a suitable level. This can only be done for "derivative" designs where such experience is available; the accuracy of *ab initio* predictions for a brand new design is at present insufficient to guarantee a suitable turbine blade life. This leads to turbine design being an iterative process with a great deal of "tuning" based on engine thermal paint tests which are both expensive and time-consuming. CFD code development must therefore aim to characterise the heat transfer effects of each element of the flow unsteadiness so that algorithms can be developed to predict heat transfer utilising the *predicted* flow field. This can only be done if one can distinguish between three-dimensional effects, rotational effects, and effects due to NGV-induced flow disturbances.

The Oxford Isentropic Light Piston Tunnel (ILPT) was initially configured with a linear cascade working section; heat transfer was measured to blade aerofoils both at a variety of turbulence levels (Nicholson, 1981), and with a moving bar upstream to produce a simulation of NGV wakes entering the blade passage (Doorly and Oldfield, 1985, Ashworth, 1987. and Johnson et al, 1988). It was subsequently converted into the rotating, fully annular facility described above, which has been used to measure blade surface pressures (Dietz and Ainsworth, 1992) and heat transfer rates (Hilditch and Ainsworth, 1990) in the rotating environment and to compare them with cascade data. A general arrangement of the facility is shown in Figure 1. These "forwards" rotation experiments, however, necessarily included wake passing, shock wave passing, secondary flows and rotational effects and, although some heat transfer features were easily identifiable in terms of wake events, it has proved difficult to resolve the discrete response to each of these features from the combined response that was actually measured.

The present experiment was designed to measure heat transfer to rotating turbine blades *without* any flow unsteadiness so that the accuracy of the time-steady rotating and secondary flow terms in the CFD codes of interest could be confirmed. This has been

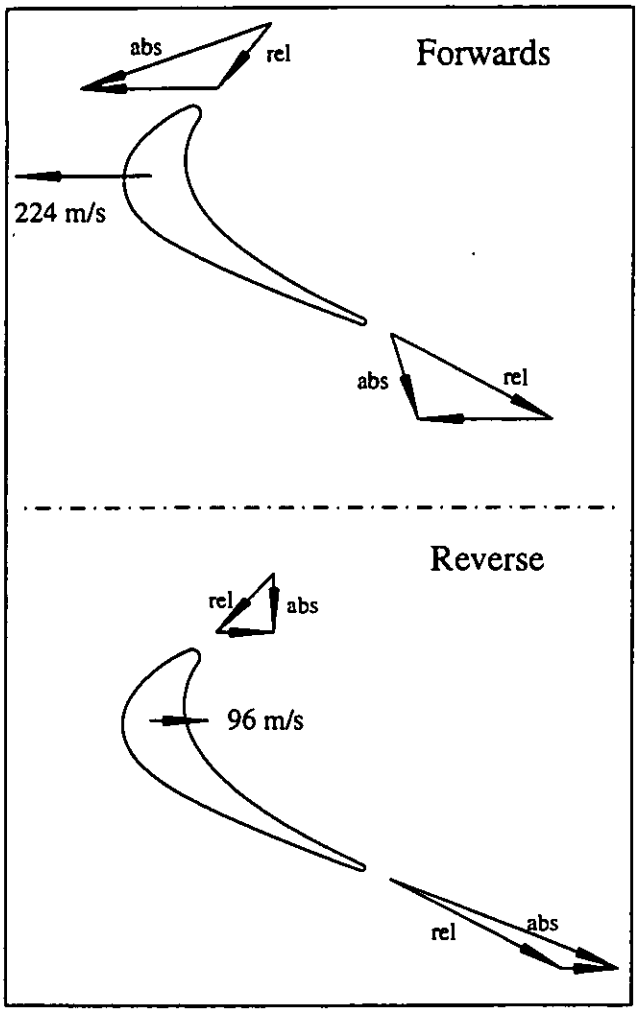

FIGURE 2. VELOCITY TRIANGLES FOR FORWARDS AND REVERSE ROTATION.

achieved by removing the nozzle guide vanes: the correct incidence onto the rotating blades is obtained by rotating the turbine in the "reverse" direction, as shown by the velocity triangles in Figure 2. The turbine thus decelerates during a run, and must be spinning at above the required test speed before the tunnel is fired. The secondary flows have, in theory, no unsteady component and, although they will be different to the forwards-rotation case, should be easily predictable by steady-state CFD codes. The blade profiles are the same as used in the forwards rotation experiment.

EXPERIMENTAL FACILITY.

The facility consists of a 0.5 m diameter shroudless turbine which is supplied with air from a piston tube. The piston tube is initially pressurised; high pressure air then enters behind a free-sliding piston, which compresses the charge towards the turbine end of the tube. When the pressure and temperature have reached suitable conditions (to provide realistic engine Mach and

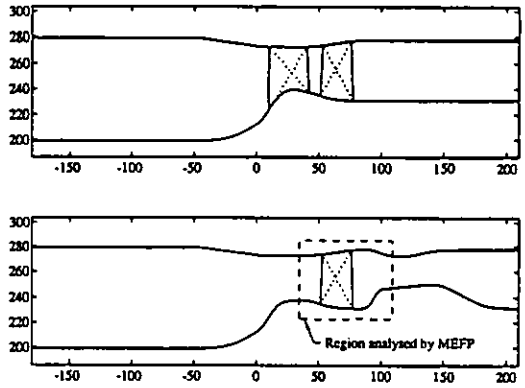

FIGURE 3. COMPARISON OF TURBINE STAGE ANNULUS FOR FORWARDS ROTATION (TOP) AND FOR REVERSE ROTATION. DASHED BOX SHOWS REGION USED IN CFD CALCULATIONS.

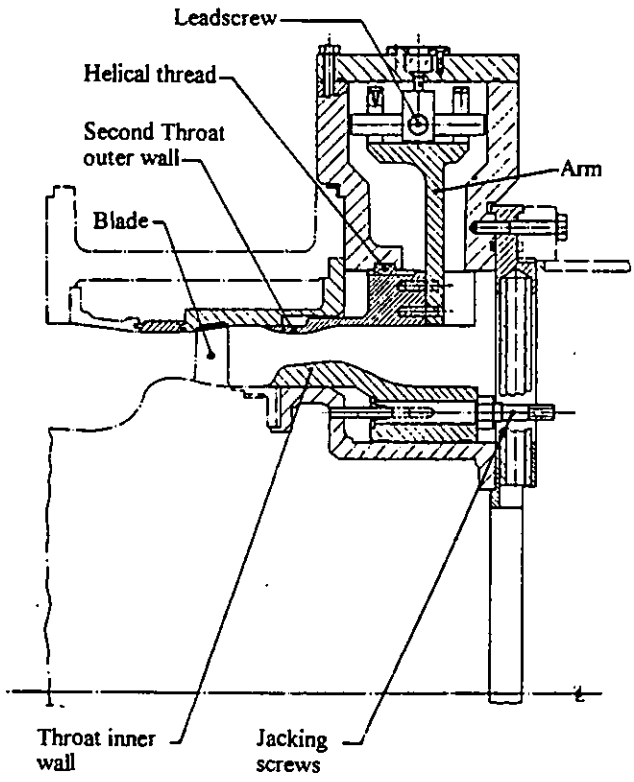

FIGURE 4. CROSS-SECTION OF SECOND THROAT, SHOWING ADJUSTMENT MECHANISM.

Reynolds numbers) a fast-acting annular gate valve opens and the air passes through the turbine and into an evacuated dump tank. The turbine is initially rotating at a speed close to the design point; it is unbraked, and accelerates rapidly through the design speed during the 200 ms run time. A slip ring allows measurements to be taken from transducers mounted on the

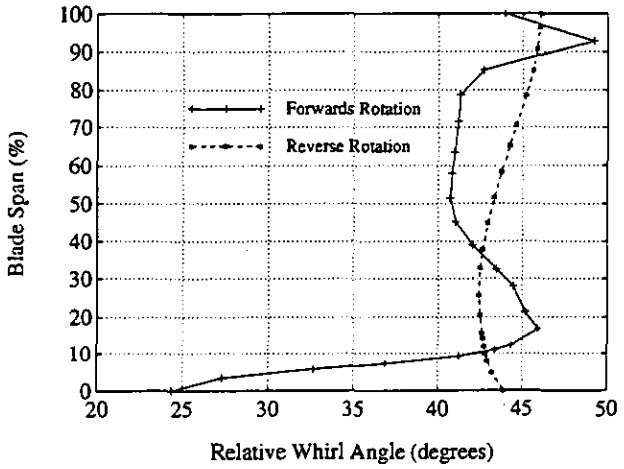

FIGURE 5. COMPARISON OF BLADE RELATIVE INLET WHIRL ANGLES FOR FORWARDS AND REVERSE ROTATION EXPERIMENTS.

blades.

The turbine annulus was redesigned for use without nozzle guide vanes so as to provide (as far as possible) a similar inlet velocity profile to the forwards rotation case and to prevent shock waves from the exhaust section propagating upstream and impinging on the blades. Figure 3 shows the annulus diagrams used in the design of the forwards and reverse rotation experiments, as described for through-flow analysis; the step expansion seen in Figure 1 has been omitted to improve convergence. The forwards rotation experiment used an adjustable "throttle plate" to set the blade exit Mach number, and had a step expansion to isolate the blade row from downstream disturbances. The second throat was redesigned for the current experiment in which the rotor absolute exit velocity is supersonic. The throat chokes the flow in the axial direction and prevents shock waves due to downstream disturbances from propagating upstream. The throat cross-sectional area sets the stage pressure ratio (as a function of dimensionless speed $\frac{N}{\sqrt{\gamma RT}}$), and is adjusted to obtain the design point rotor exit Mach number at the design speed.

The second throat was initially designed using an axi-symmetric streamline curvature method, and subsequently analysed using PHOENICS to confirm that the throat would choke at the design conditions in the presence of supersonic swirl velocities. Variation of the flow area is achieved by constructing the throat with sliding sections in both the annulus walls. Coarse adjustment of the area is achieved by positioning the inner wall of the throat using jacking screws, with the dump tank disconnected to provide access. Fine adjustment is then possible by rotating a section of the outer wall; as it rotates, a helical thread around the inside of the outer annulus wall pushes it axially while ensuring that it does not tilt. The thread is constructed from PTFE (similar to Teflon™) rods to minimise friction, and the lip where the two annulus sections touch is machined to a sharp edge to avoid any step which might affect

TABLE 1. CHANGES IN DESIGN POINT CONDITIONS REQUIRED FOR REVERSE ROTATION.

	Forwards	Reverse
Rotor exit Reynolds number Re_{Cax}	1.554×10^6	1.426×10^6
NGV exit Mach number	0.946	N/A
Rotor relative exit Mach number	0.959	0.959
Shaft speed rpm	8434	-3600
Inlet total temperature, K	374.4	331.7
Inlet total pressure, Pa	8.02×10^5	4.6×10^5
Blade axial chord C_{ax} mm	24.35	24.35
Mass flow rate, kg/s	29.1	28.7
Temperature ratio $T_{g,rel}/T_w$	1.141	1.141

the flow. A cross section of the system is shown in Figure 4.

Figure 5 compares the blade incidence angles for the forwards and reverse rotation tests. The new design point has been chosen to keep the incidence angles over the central sections of the blade at their former levels; a complete simulation of inlet angles over the full annulus height is not possible. Design point conditions and non-dimensional parameters for the two cases are shown in Table 1.

Seven turbine blades were instrumented with thin-film heat flux gauges. The blades are made from a nimonic alloy which is coated with an insulating enamel layer. Five blades had gold paint gauges, photoetched to give a serpentine pattern. These are approximately 1 mm square, which does not give sufficient resolution to show turbulent fluctuations within the boundary layer. The other two blades were made for the present experiment with a series of 15 hand-painted platinum gauges which are 5 mm long but only 0.25 mm wide in the circumferential direction. The gauge signals are boosted by an in-shaft amplifier before passing through slip rings to a 12-bit analogue to digital convertor. The in-shaft amplifier includes a feedback circuit which varies the gain from 5.2× at DC to 420× at 90 kHz to improve the signal to noise ratio of the small amplitude high frequency components of the gauge signal and allow them to be digitised (Ainsworth et al, 1988b). The gain is set by a simple resistor-capacitor network and can be accurately predicted so that, once digitised, the effect of the amplifier can be removed by suitable processing.

Digital signal processing techniques are used to convert this data into accurate heat fluxes, taking measured calibration parameters for each gauge and allowing for local variations in the thickness and properties of the enamel substrate. The heat flux signals are finally converted to Nusselt numbers, and the mean level over the period when the shaft speed was within 100 rpm of the design value is calculated. The Nusselt number is calculated as

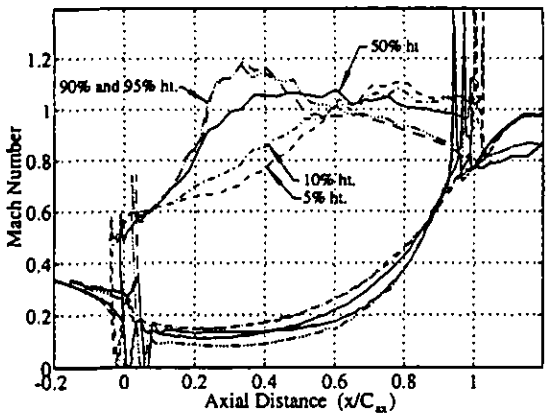

FIGURE 6. MEFP PREDICTION OF BLADE SURFACE MACH NUMBERS.

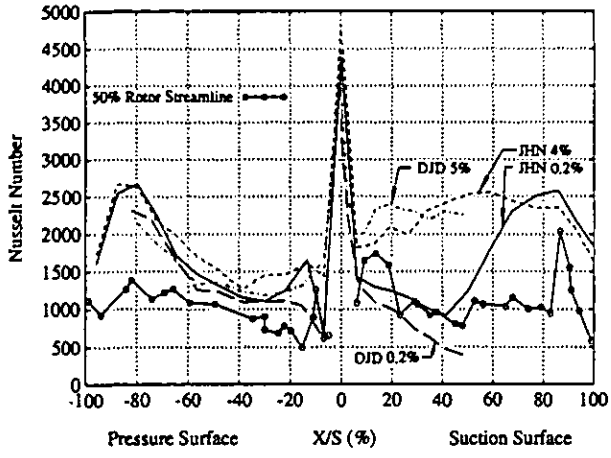

FIGURE 7. COMPARISON OF REVERSE ROTATION MEASUREMENTS WITH CASCADE DATA, JHN(1981) AND DJD(1985), AT VARIOUS FREESTREAM TURBULENCE INTENSITIES.

$$Nu = \frac{\dot{q}}{T_{0,rel} - T_w} \frac{C_{ax}}{k_w}$$

and the experimental error is of the order of ±5 %.

Close examination of the high-frequency heat flux signals showed that there was a slight cyclic fluctuation despite the absence of nozzle guide vanes. This was caused by the struts of the annular gate valve, with 32 cycles per revolution; it appears that the heat transfer effect is due to a slight spatial variation in air temperature as a result of heat loss to the struts, rather than being due to a velocity-deficit wake interacting with the blade boundary layer. The rms amplitude is typically only 3% of the mean level and the fluctuations were successfully removed by high-pass filtering, with a cut-off frequency of 4 kHz, to give a clearer impression of the turbulent structure of the boundary layer.

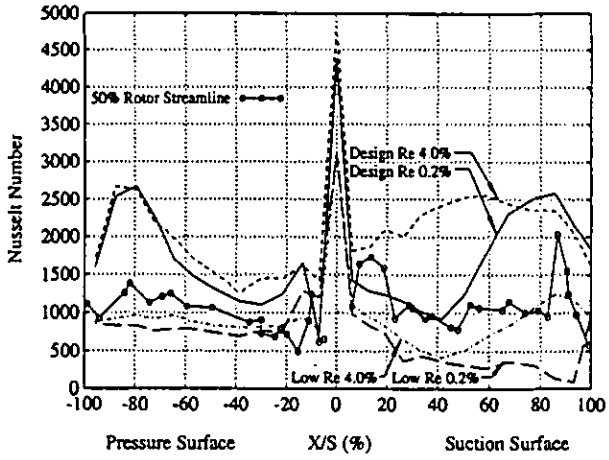

FIGURE 8. COMPARISON OF REVERSE ROTATION DATA WITH CASCADE DATA AT VARIOUS REYNOLDS NUMBERS.

CFD PREDICTION METHODS.

The flow through the reverse-rotation turbine was analysed using the Moore Elliptic Flow Program "MEFP" (Moore and Moore, 1985, 1989), which is a three-dimensional viscous flow solver using a finite volume pressure prediction/correction algorithm. At a fundamental level it is therefore similar to the Phoenics code used for the facility design, and conceptually different to CFD codes that use a time-marching algorithm. Whereas Phoenics is a general purpose program however, MEFP is designed specifically for the solution of turbomachinery flows. The three-dimensional grid may be specified in either cylindrical or spherical coordinates and can handle arbitrary shapes because it does not require rectangular cells.

The generation of accurate solutions by a viscous flow program is always dependent on the suitability of the turbulence model by which the effect of turbulence on shear stresses within the flow is estimated. MEFP calculates an effective viscosity in terms of laminar and turbulent components. The laminar component is simply the dynamic viscosity of the air; the turbulent component is based on a two layer eddy viscosity model which treats shear layers as having "inner" and "outer" layers. In the inner region the turbulent viscosity is calculated using a Prandtl-van Driest viscosity model, and in the outer part a mixing length formula is used (Baldwin and Lomax, 1978). Outside any shear layers, the program assumes that the freestream turbulence intensity and length scale are fixed at their inlet values and do not vary with position or velocity.

Flow parameters for MEFP are defined in the rotor-relative frame. The relative stagnation pressure and temperature, inlet velocity and inlet static pressure distribution were specified, together with a fixed exit static pressure. Radial pressure profiles were derived from the streamline curvature design program mentioned above. The exit plane was chosen to be before the second throat to avoid possible convergence problems if two throats were present. The input conditions did not include a boundary layer on the annulus walls.

Several different computers were required for the analysis. A proprietary Rolls-Royce code for Silicon Graphics workstations was used for grid generation and output processing; the grid was transferred to a mainframe at Rolls-Royce to generate appropriate boundary conditions, and MEFP itself was then run on a Convex machine.

Two calculations were done. A coarse grid of 85(axial)× 27(pitchwise)×30(spanwise) grid points was initially used to check convergence and provide aerodynamic input data for the fine grid case. A finer grid of 107×41×36 points was then used for the heat transfer calculation. The grid is of "H" form and defines a single blade to blade passage, including the aerofoil itself; there are actually 65 stations between leading and trailing edges and 28 across the passage between pressure and suction surfaces. The near-wall points were at 0.006 mm from the surface, and the maximum grid expansion factor was 2. The boundary conditions were chosen to achieve repeatability between passages around a notional complete annulus. The axial extent of the grid is shown by the box in Figure 3.

The state of the blade surface boundary layers had to be specified explicitly because MEFP cannot at present predict transition; this was done by entering an intermittency distribution over the blade surface. Four different combinations of intermittency and free-stream turbulence were tried in an attempt to study the sensitivity to input parameters and to identify a boundary layer state that would closely match the experimental data. In three of these cases the boundary layers were defined as being fully turbulent over the whole surface, with turbulence intensities of 0.5%, 1% and 2% respectively. The fourth case used an intermittency distribution predicted by a 2-D boundary layer code (Forest, 1978) which was turbulent over the pressure surface, and on the suction surface rose from 0 at the leading edge to 0.096 at the trailing edge. The suction surface distribution may be empirically correlated using the formula $\sigma = 0.207(X/S)^3 - 0.14(X/S)^2 + 0.0306X/S - 0.0004$ with a maximum error of 0.002. This "transitional boundary layer" case used a freestream turbulence intensity of 1%. In each case the fractional turbulence intensity was assumed constant throughout the grid.

The blade surface Mach number distributions predicted by MEFP are shown in Figure 6. This calculation assumed a turbulence intensity of 1%; the predicted velocity distribution is, however, insensitive to turbulence intensity and intermittency distribution apart from slight blockage effects on the suction surface at root and tip due to changes in boundary layer thickness. The blade profile is parallel ruled (i.e. not twisted) so the changes in inlet angle in Figure 5 correspond to changes in the angle of incidence from root to tip. This causes the trend seen in Figure 6 of a fall (from root to tip, with spanwise location expressed as % height) in pressure surface velocity and an increase in velocity on the suction surface crown.

RESULTS.

Experimental mid-height Nusselt numbers.

Figure 7 compares the measured mean Nusselt numbers at the mid-height streamline with data previously taken using 2-D cascades in the ILPT, with the same aerofoil profile, by J.H.Nicholson (1981, identified as "JHN") and D.J.Doorly et al (1985a & b, identified as "DJD"). Nicholson used a seven blade cascade with C_{ax} = 33.7 mm, while Doorly used a four blade cascade with C_{ax} = 51.9 mm. These cascade tests both studied the effects of variations in freestream turbulence; Doorly subsequently used a rapidly moving bar to generate simulated NGV wakes, though the data presented here is with grid-generated turbulence only. They are therefore directly comparable to the present data.

Over the first half of the suction surface the rotor data agrees well with the cascade studies. The inlet turbulence level to the rotor has been estimated to be 0.5% and one can see that the level is generally close to Nicholson's data with 0.2% turbulence. Over the second half of the suction surface Nicholson's cascade data shows an increase in Nusselt number as transition occurs. The rotor Nusselt number distribution remains fairly constant over the second half of the suction surface before rapidly rising towards Nicholson's turbulent level as transition occurs near the trailing edge; the Nusselt numbers then fall, in a similar manner to the cascade data, as the turbulent boundary layer thickens. Doorly's data did not extend as far as the trailing edge, but over the forward part of the suction surface he measured lower Nusselt numbers than Nicholson and on this basis, had he taken data on the rear suction surface, it might be expected to have been close to the rotor data shown here. The sensitivity of the cascade data to experimental conditions means that one cannot determine whether or not rotational effects are of importance here.

On the pressure surface, both the rotor and cascade studies show a dip at X/S=4% followed by a peak at the 10% position. Doorly et al (1985) describe the presence of a separation bubble on the pressure surface at X/S=4%, with reattachment at the peak position. The boundary layer was thought to probably be transitional from X/S = 20% to 60%, and turbulent thereafter. Once transition has started the boundary layer is not expected to be sensitive to small amounts (<5%) of freestream turbulence, and this is confirmed by the cascade data.

The Reynolds numbers in the cascade tests (Nicholson's and Doorly's data) were approximately 9% higher than in the reverse rotation tests. The effects of changes in Reynolds number can be seen in Figure 8, which shows data by Nicholson both at the design Reynolds number, $Re_{C_{ax}} = 1.55\times10^6$, and at a lower (50% of design) Reynolds number condition. It can be seen that the low Reynolds number tests produced values closer to the present data, suggesting that the known Reynolds number differences, while not so large as those between Nicholson's conditions, may in part explain the pressure surface discrepancies in Figure 7. Such a Reynolds number difference might be expected, if one assumes a turbulent correlation of the form $Nu \propto Re^{0.8}$, to change Nusselt numbers by 7%. This would bring the cascade and rotor data very close together between X/S = 30% and 70% and would lengthen the transitional region. The larger discrepancies in rotor Nusselt number at X/S = 15% and 80% may be due to rotational phenomena affecting the separation bubble and (together with Reynolds number effects) the length of the transitional region.

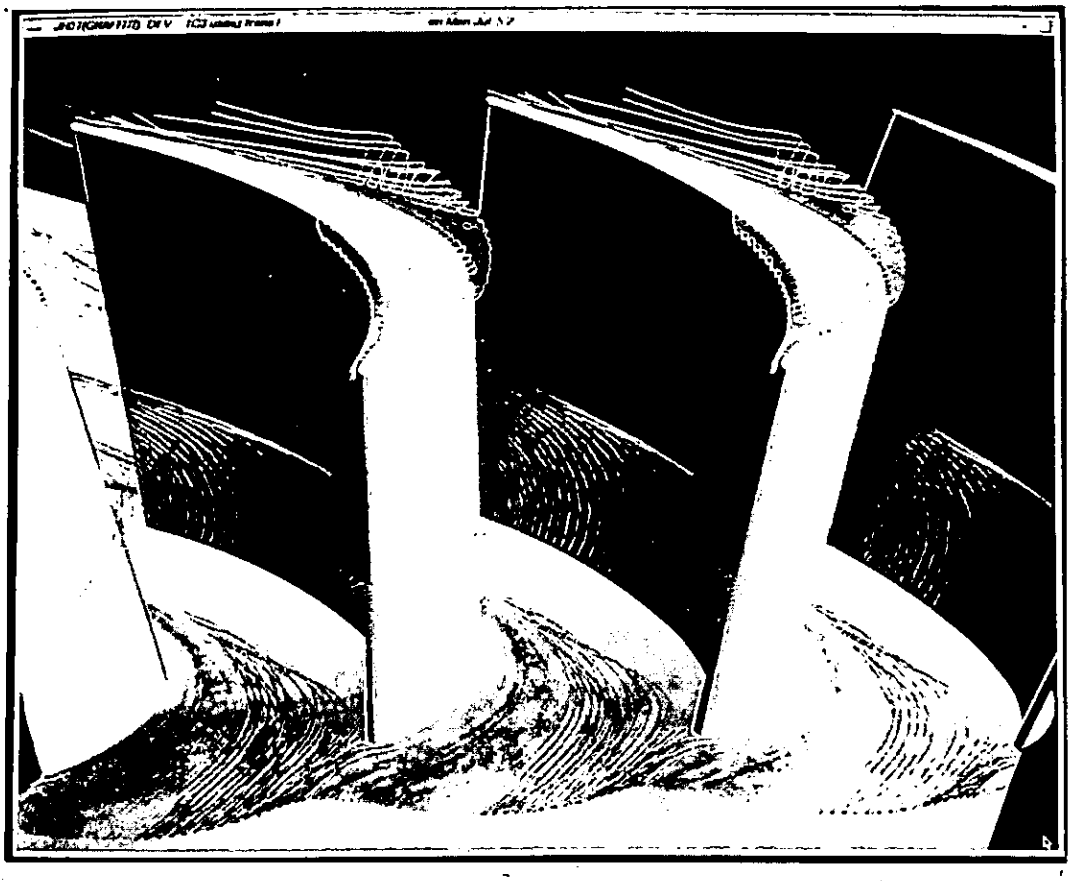

FIGURE 9. SECONDARY FLOW AND OVER-TIP STREAMLINES PREDICTED BY MEFP.

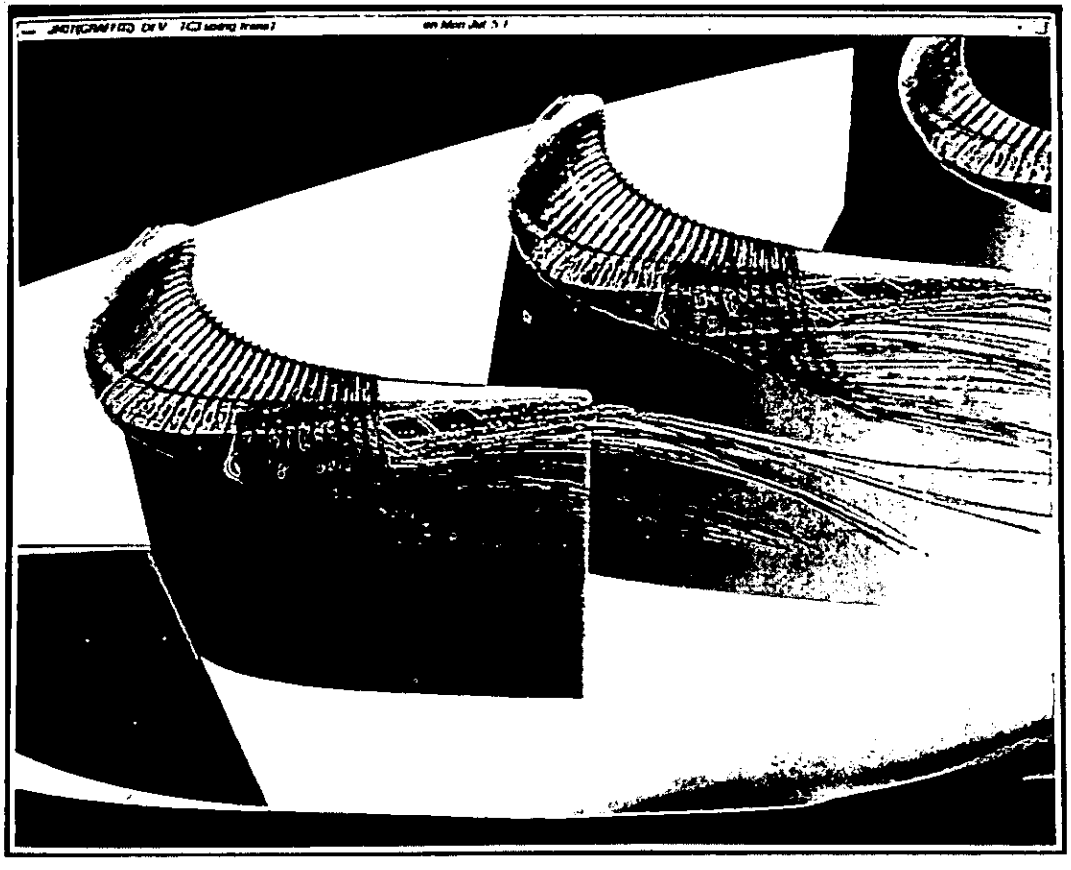

FIGURE 10. PREDICTED OVER-TIP FLOW SEEN FROM DOWNSTREAM.

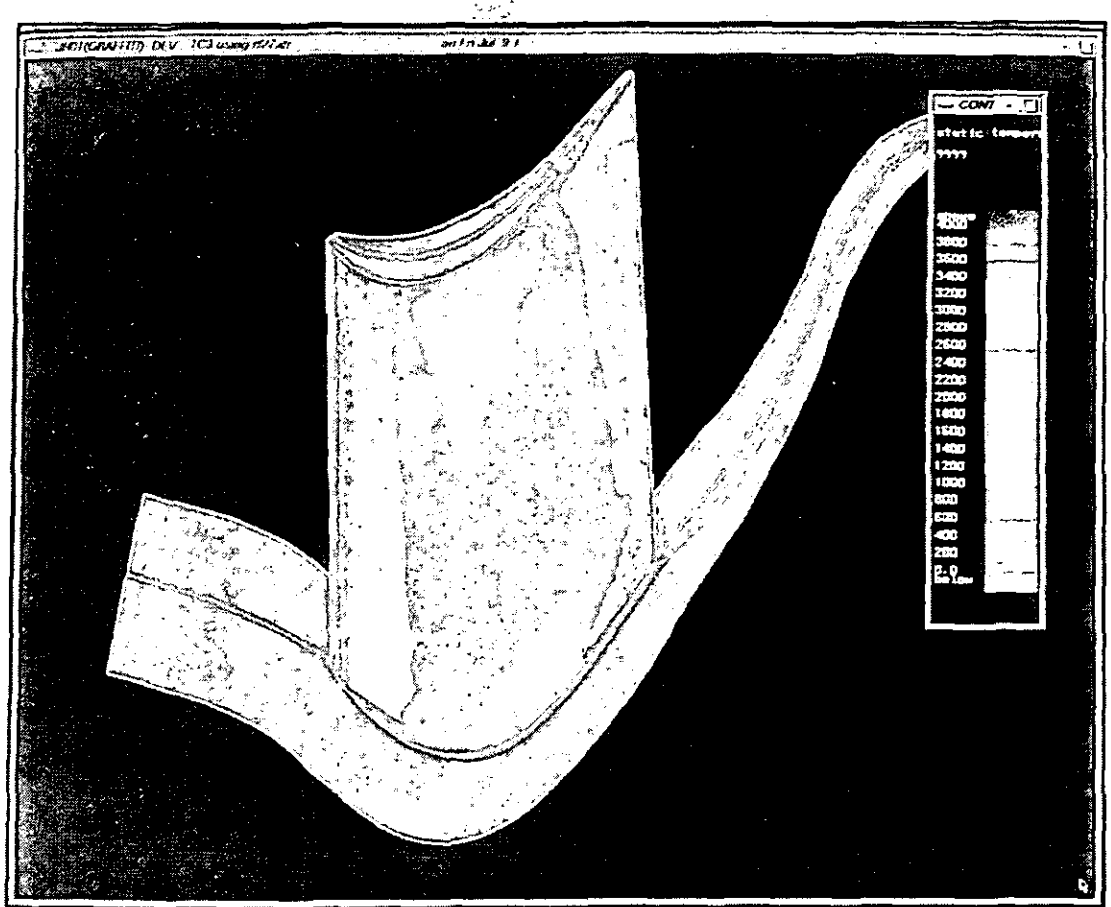

FIGURE 11. MEFP PREDICTION OF NUSSELT NUMBERS ON BLADE SUCTION SURFACE (TRANSITIONAL INTERMITTENCY DISTRIBUTION).

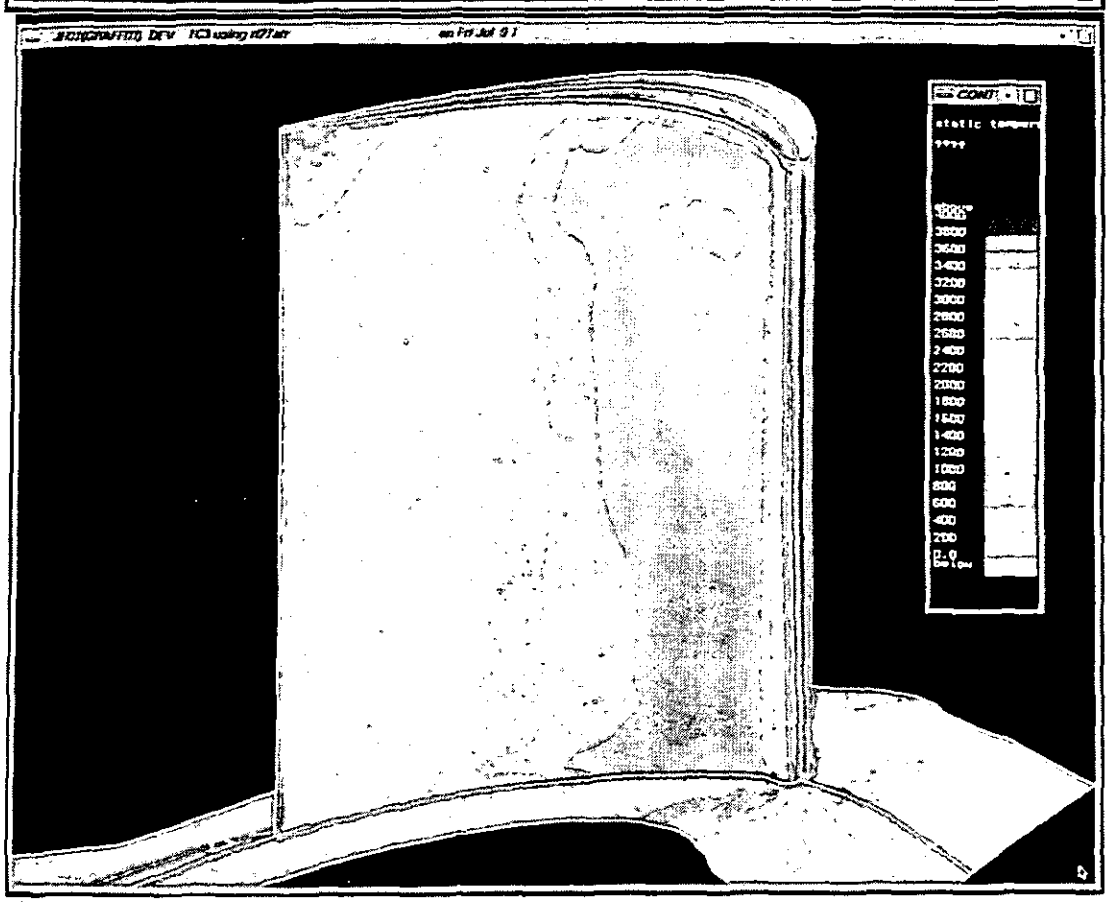

FIGURE 12. MEFP PREDICTION OF NUSSELT NUMBERS ON BLADE PRESSURE SURFACE (TRANSITIONAL INTERMITTENCY DISTRIBUTION).

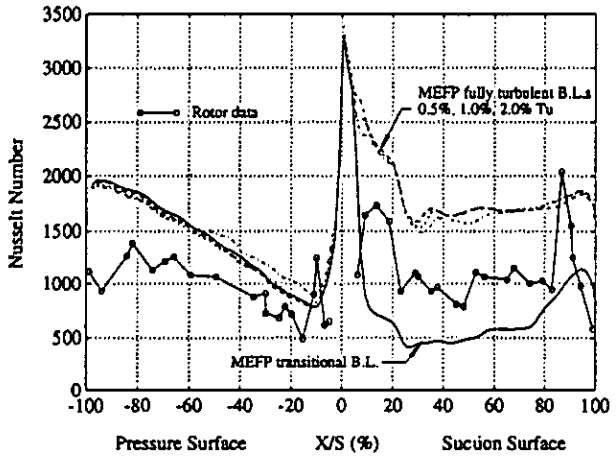

FIGURE 13. COMPARISON OF MEFP PREDICTION WITH REVERSE ROTATION DATA AT MID-HEIGHT.

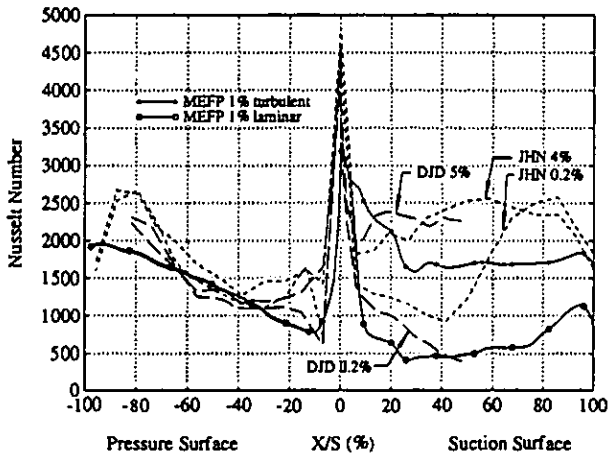

FIGURE 14. COMPARISON OF MEFP PREDICTION OF MID-HEIGHT NUSSELT NUMBERS WITH CASCADE DATA.

CFD predictions.

The effectiveness of MEFP in modelling three-dimensional viscous flows is illustrated by Figure 9, which shows computed particle paths for flows on the inner platform, at mid-height and in the over-tip regions. The secondary flows on the platform are clearly visible, and in Figure 10 the vortex produced by the tip leakage flows can also be seen. The tip gap is 0.5 mm (Sheard, 1990) and the blade tip is a smooth, cylindrical surface.

Figure 11 shows contours of MEFP-predicted Nusselt number on the blade suction surface with the "transitional" intermittency distribution. There is a fall in heat transfer from the leading edge towards the crown, followed by a slight rise as the intermittency increases towards the trailing edge. The distribution is remarkably two-dimensional and has little spanwise variation apart from the crown having patches of low heat flux in the root and tip regions where cool secondary flow fluid passes onto the surface.

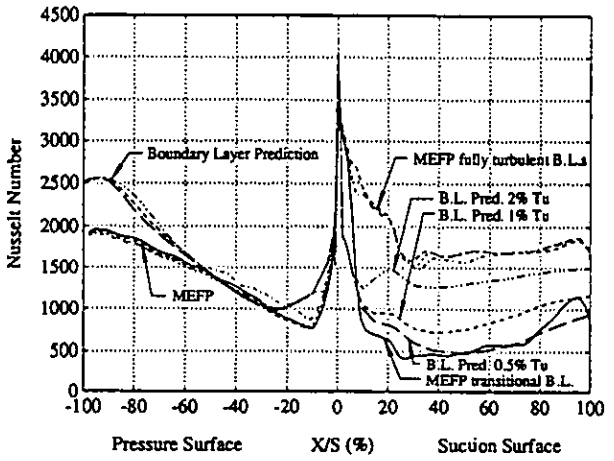

FIGURE 15. COMPARISON OF MEFP MID-HEIGHT PREDICTION WITH 2-D BOUNDARY LAYER CODE.

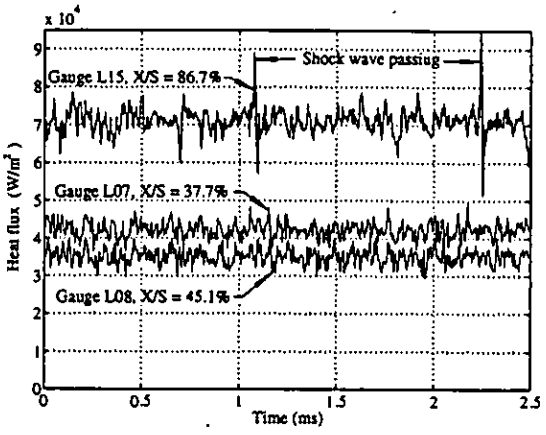

FIGURE 16. SHOCK WAVE PASSING ON REAR SUCTION SURFACE. OTHER GAUGES ARE FREE FROM INTERFERENCE.

Figure 12 shows the pressure surface Nusselt number distribution. There is a cool patch on the early pressure surface at 80% span, which is perhaps caused by low velocities here resulting from the change in incidence mentioned above. The tip region has a hot spot over the last 15% chord, which must be due to the boundary layer thinning as it is drawn into the over-tip leakage flow.

Figure 13 compares the reverse rotation data with an MEFP prediction of Nusselt numbers at mid-height. On the suction surface there is a great difference between the MEFP predictions with turbulent boundary layers and that with a transitional boundary layer, with the experimental data about half-way between the two. It is clear that some way of accurately predicting the boundary layer state is essential if accurate predictions in this region are to be achieved. On the pressure surface, however, the choice of boundary layer state has little effect on the prediction, which is approximately 25% above

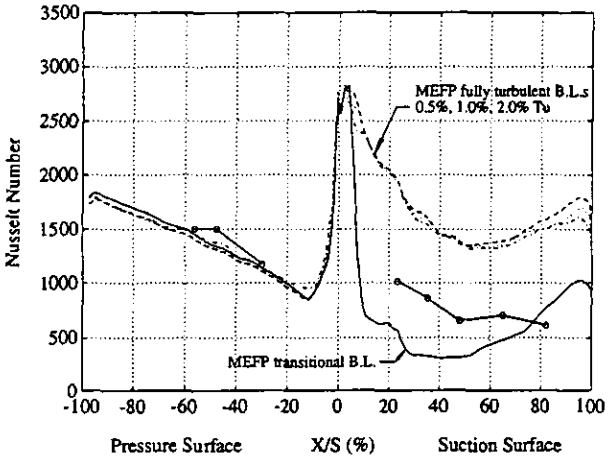

FIGURE 17. COMPARISON OF MEFP PREDICTION WITH MEASURED REVERSE ROTATION NUSSELT NUMBERS AT 10% SPAN.

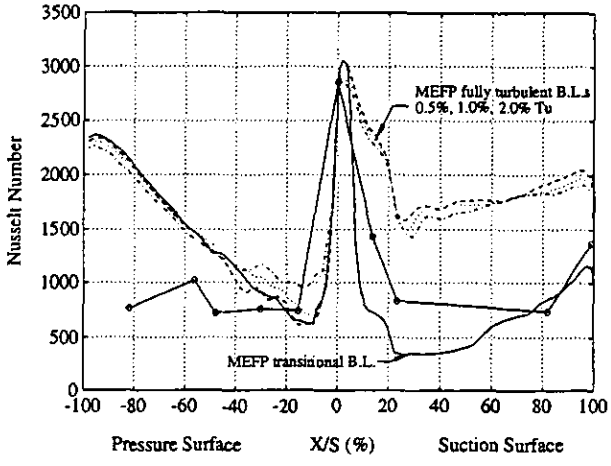

FIGURE 18. COMPARISON OF MEFP AND MEASURED REVERSE ROTATION NUSSELT NUMBERS AT 90% SPAN.

measured levels.

Figure 14 compares two MEFP reverse rotation predictions, with 1% freestream turbulence and either laminar or turbulent intermittency distributions, with the cascade data from Figure 7. On the suction surface the laminar portion of both Doorly's and Nicholson's data lies between the two MEFP solutions; the turbulent region, however, lies considerably above the turbulent prediction even with only 0.2% freestream turbulence. The pressure surface shows much better agreement although the prediction is still approximately 35% low in the X/S = 20% and 80% regions.

Figure 15 shows a prediction from the 2-D boundary layer code (Forest, 1978). The 3-D prediction (MEFP) shows a slower rise in heat transfer along the pressure surface than the 2-D code and so (with reference to Figure 13) is closer to the experimental data. On the suction surface, the fully turbulent MEFP predictions lie above the two-dimensional prediction; at no point does the intermittency predicted by the 2-D code rise above 50%, and this leads to lower heat fluxes than if it had become fully turbulent. When MEFP is run using the intermittency distribution predicted by the 2-D code for 0.5% turbulence, the resulting "transitional boundary layer" line is in fact close to the 2-D prediction.

Fast response heat flux measurements.

Heat transfer data was captured at 200 kHz in an attempt to determine the boundary layer state. On the suction surface, heat transfer spikes were visible at the $X/S \approx 86.7$ and 90.4% gauges due to shock wave passing (Figure 16). Shock waves have been seen on the rear suction surface of this aerofoil in previous Schlieren tests (Doorly and Oldfield, 1985), and the effect of slow oscillations of the driving piston is to make the shock waves pass over the gauges as the exit Mach number varies. The fact that the other gauges included in Figure 16 for comparison do not show the same spikes proves that the signals are genuine and are not due to electrical interference.

The pressure surface fast heat transfer signals also showed very little modulation. Despite indications from the time-mean Nusselt numbers (Figure 7) that the boundary layer might possibly be transitional, on neither surface was there any signal suggesting a transitional boundary layer, nor was it possible to obtain any significant (>0.2) correlation between signals from successive gauges. Doorly found the suction surface to be laminar at 0.4% Tu, transitional at 2% Tu, and to undergo rapid transition at 4.5% Tu, and the transitional fluctuations in heat flux were easily visible. The present aerofoils are, however, smaller than Doorly's and it is possible that the instrumentation frequency response is insufficient to show such details.

Root and tip data.

Figure 17 compares reverse rotation measurements at 10% span with the MEFP prediction at this section. On the pressure surface the predicted value is close to the mid-height value. The measured Nusselt numbers are approximately 50% above the mid-height values, and the prediction is in better agreement here than at mid-height. On the suction surface the predicted Nusselt numbers are 10-20% lower than at mid-height, which may be due to the horseshoe vortex entraining endwall fluid and thickening the boundary layer here. As at mid-height, the suction surface measurements lie between the predicted transitional and turbulent levels.

One would expect the passage vortex resulting from reverse rotation to strengthen secondary flows on the inner platform, and to weaken them on the outer annulus wall; and, in general, one would expect secondary flows to thin the pressure surface boundary layer in the root and tip regions, and to thicken the suction surface layer. On the outer wall in the reverse rotation case the relative motion of the wall will oppose the secondary flow and this might actually lead to thicker boundary layers in the pressure surface tip region if the over-tip leakage is insufficient to remove the endwall boundary layer.

Comparing the experimental data in Figure 17 with the mid-

height values in Figure 13 shows some evidence of secondary flow effects, in that the root measurements have higher pressure surface and lower suction surface values than at mid-height.

Figure 18 shows the corresponding data at 90% span. The predicted pressure surface level is close to the mid-height value until *X/S*=60%, when it rises more rapidly; as mentioned above, this may be due to a thinning of the boundary layer resulting from the over-tip leakage. The experimental data is lower than at mid-height which suggests that the mechanism discussed above in which the convected endwall boundary layer leads to lower pressure surface heat transfer is actually occurring; conversely, one may infer that MEFP has over-predicted the tip leakage flow.

On the suction surface there are only a limited number of experimental points, but they do show very similar Nusselt numbers to the mid-height gauges. The MEFP prediction is very similar to that at mid-height; although the predicted levels differ from the measured data, it is encouraging that the trends in heat transfer when comparing different spanwise sections are similar to those seen experimentally.

CONCLUSIONS.

An innovative technique for testing turbine blades in a rotating environment without the complexity of unsteady flows has been demonstrated and found to provide valuable data for CFD evaluation.

The experimental mid-height Nusselt numbers are 20-50% lower than cascade measurements on the early and late pressure surface. This is thought to be due to a combination of rotational and Reynolds number effects on the boundary layer. The mean Nusselt number level, together with cascade measurements by Doorly (1985), suggests that this boundary layer should be transitional, but the fast response data is unable to confirm this. On the suction surface the cascade data is very sensitive to the inlet conditions and one cannot draw any reliable conclusions about the difference between the static and rotating experiments.

Comparing MEFP predictions of the reverse rotation flow against experimental measurements shows that pressure surface heat transfer is over-predicted by approximately 30%; the prediction is, in fact, closer to 2-D cascade Nusselt numbers. On the suction surface the solution is very dependant on the intermittency distribution chosen. Possible solutions straddle the experimental points, but are either 50% high (turbulent) or 50% too low (transitional). When comparing equivalent predictions, the general trends in heat transfer are similar to those seen in the test data, despite the uncertainty in the actual level. Further work is required to find an intermittency distribution that mirrors the experimental data and to determine whether this is physically realistic.

Comparison of MEFP with a 2-D boundary layer code shows MEFP to be closer to the measured data on the pressure surface, while on the suction surface the 2-D code is, at present, at least as good as the 3-D prediction.

Root and tip measurements show differences in level between the cascade and rotating experiments that can be explained qualitatively in terms of rotational, three-dimensional and over-tip leakage phenomena. It also appears from a comparison of the tip-section heat fluxes with the MEFP prediction that the latter may have over-predicted the effects of over-tip leakage relative to the test case.

ACKNOWLEDGEMENTS.

The idea of reversing the direction of turbine rotation and removing the nozzle guide vanes was originally proposed by Mr G. Dailey of Rolls-Royce Derby. The authors are grateful to Rolls-Royce plc and the SERC for funding this work, and would like to thank all the Rolls-Royce personnel who have assisted with running CFD and output processing software.

REFERENCES.

Ainsworth, R.W., Schultz, D.L., Davies, M.R.D., Forth, C.J.P., Hilditch, M.A., Oldfield, M.L.G. and Sheard, A.G., *A Transient Flow Facility for the Study of the Thermofluid Dynamics of a Full Stage Turbine under Engine Representative Conditions*. ASME 88-GT-144.

Ainsworth, R.W., Allen, J.L., Davies, M.R.D., Doorly, J.E., Forth, C.J.P., Hilditch, M.A., Oldfield, M.L.G., and Sheard, A.G., *Developments in Instrumentation and Processing for Transient Heat Transfer Measurement in a Full Stage Model Turbine*, ASME Journal of Turbomachinery Vol. 111 pp20-27, January 1989.

Ashworth, D.A., LaGraff, J.E., and Schultz, D.L, *Unsteady interaction effects on a transitional turbine blade boundary layer*, Proc. 2nd Joint ASME/JSME Thermal Engineering Joint Conference, March 1987.

Baldwin, B.S., and Lomax, H., *Thin layer approximation and algebraic model for separated turbulent flows.* AIAA Paper 78-257, 1978.

Dietz, A.J., and Ainsworth, R.W., *Unsteady Pressure Measurements on the Rotor of a Model Turbine Stage in a Transient Flow Facility.* ASME 92-GT-156.

Doorly, D.J. and Oldfield, M.L.G., *Simulation of the effects of shock passing on a turbine rotor blade.* ASME 85-GT-112, 1985.

Doorly, D.J., Oldfield, M.L.G., and Scrivener, C.T.J., *Wake Passing in a Turbine Rotor Cascade.* AGARD CP390.

Forest, A.E., *Engineering Predictions of Transitional Boundary Layers*, AGARD CP224, 1978.

Hilditch, M.A., and Ainsworth, R.W., *Unsteady Heat Transfer Measurements in a Rotating Turbine Stage,* ASME 90-GT-175, Brussels, 1990.

Johnson, A.B., Rigby, M.J.G., Oldfield, M.L.G., Ainsworth, R.W., and Oliver, M.J., *Surface Heat Transfer Fluctuations on a Turbine Rotor Blade due to Upstream Shock Wave Passing,* ASME 88-GT-172.

Moore, J.G. and Moore, J., *Calculation of viscous flow using the Moore Elliptical Flow Program.* Turbomachinery Research Group Report JM/85-4, Virginia University and Institute of Technology, 1985.

Moore, J.G. and Moore, J., *Moore Elliptic Flow Program*

(MEFP). User Guide, Virginia University and Institute of Technology, 1989.

Nicholson, J.H., *Experimental and theoretical studies of the aerodynamic and thermal performance of modern gas turbine blades*. DPhil Thesis, University of Oxford, 1981.

Sheard, A.G., and Ainsworth, R.W., *Aerodynamic and mechanical performance of a high pressure gas turbine stage in a transient wind tunnel*, ASME 90-GT-253, 1990.